

Non-equilibrium scenarios in cluster-forming quantum lattice models

Adriano Angelone*,^{1,2} Tao Ying*,³ Fabio Mezzacapo,⁴ Guido Masella,⁵ Marcello Dalmonte,^{1,2} and Guido Pupillo⁵

¹*Abdus Salam ICTP, Strada Costiera 11, I-34151 Trieste, Italy*

²*SISSA, Via Bonomea 265, I-34136 Trieste, Italy*

³*Department of Physics, Harbin Institute of Technology, 150001 Harbin, China*

⁴*Univ Lyon, ENS de Lyon, Univ Claude Bernard,*

CNRS, Laboratoire de Physique, F-69342 Lyon, France

⁵*icFRC and ISIS (UMR 7006), Université de Strasbourg and CNRS, 67000 Strasbourg, France*

(Dated: September 16, 2019)

We investigate the out-of-equilibrium physics of monodisperse bosonic ensembles on a square lattice. The effective Hamiltonian description of these systems is given in terms of an extended Hubbard model with cluster-forming interactions relevant to experimental realizations with cold Rydberg-dressed atoms. The ground state of the model, recently investigated in [Phys. Rev. Lett. 123, 045301 (2019)], features, aside from a superfluid and a stripe crystalline phase occurring at small and large interaction strength V respectively, a rare first-order transition between an isotropic and an anisotropic stripe supersolid at intermediate V . By means of Quantum Monte Carlo calculations we show that the equilibrium crystal may be turned into a glass by simulated temperature quenches and that out-of-equilibrium isotropic (super)solid states may emerge also when their equilibrium counterparts are anisotropic. We find, after quenching, no evidence of coexistence between superfluid and glassy behavior. Such an absence of superglassiness is qualitatively explained.

I. INTRODUCTION

The search for ordered or disordered exotic states of matter is a very active field of investigation in condensed matter physics [1–3]. The interactions between the individual constituents of a given system play a fundamental role in this context, being intrinsically related to the physical mechanisms responsible for the stabilization of different (possibly novel) physical scenarios. Usually, intriguing equilibrium or out-of-equilibrium (OOE) properties emerge in the presence of frustration, i.e., the impossibility of simultaneously satisfying a minimum energy condition for all terms of the Hamiltonian (see, e.g., [4, 5]). The latter may arise, for example, from competing interactions, polidispersity and/or from the presence of peculiar substrates, i.e., lattices.

Recently, a large class of purely repulsive, isotropic extended-range interactions (ERI), whose relevance ranges from classical soft-matter systems [6–8] to cold Rydberg-atom experiments [9–15], has elicited considerable theoretical interest. Indeed, these potentials offer the possibility to explore a variety of equilibrium and OOE phenomena in realistic models where frustration, in the forms discussed above, is not included. The main features of (pair-wise) ERI are a plateau which extends up to inter-particle distances of the order of the critical radius r_c and a tail quickly approaching zero for $r > r_c$ [see Fig. 1(a)]. Systems with ERI at high enough particle density ρ are characterized, in the classical limit, by a so-called cluster crystalline ground state (GS) where crystalline sites are occupied by self-assembled aggregates of particles (i.e., clusters). Classical cluster crystals have been shown to possess peculiar equilibrium dynamical properties resembling those of glass-forming liquids, while still retaining structural order [16]. For these systems, OOE glassy scenarios where disorder coexists with

clusterization have also been predicted [17, 18]. Furthermore, when quantum effects are taken into account, clusterization may lead to anomalous Luttinger-liquid behavior in one spatial dimension (1D) [19–22], as well as to the coexistence of diagonal long range order and superfluidity (i.e., supersolidity) in 2D free-space [23–26] or on a triangular lattice [27]. Here, superfluidity may also be concomitant to glassiness in a so-called OOE superglass.

In order to gain theoretical insight into the novel physical phenomena related to clusterization, as well as into the interplay of the latter with quantum effects, system geometry, and interaction radius r_c , it is of crucial interest to extend the investigation to different lattices and choices of relevant parameters. In this context, a recent work by some of us [28] has been devoted to the study of the GS phase diagram of a cluster-forming model of hard-core bosons with ERI on a square lattice. For such a model the GS is a superfluid (stripe crystal) for sufficiently small (large) interaction strength V . Surprisingly, for intermediate values of V a first order phase transition occurs between two different supersolids: an isotropic one, emerging from the superfluid when V is increased, and an anisotropic stripe supersolid emerging from the partial quantum melting of the large- V , essentially classical, crystal.

The study of the GS phases mentioned above required extensive calculations and careful temperature and interaction annealings due to the presence of many competing OOE states. The nature of the latter, as well as their similarities and differences with respect to the equilibrium phases, are the focus of this work, in which we present a systematic study of the OOE scenarios of the model studied in [28]. By means of the Path Integral Monte Carlo approach, we drive the system out of equilibrium via simulated low-temperature (T) quenches, analyzing the changes that this procedure induces on the equilib-

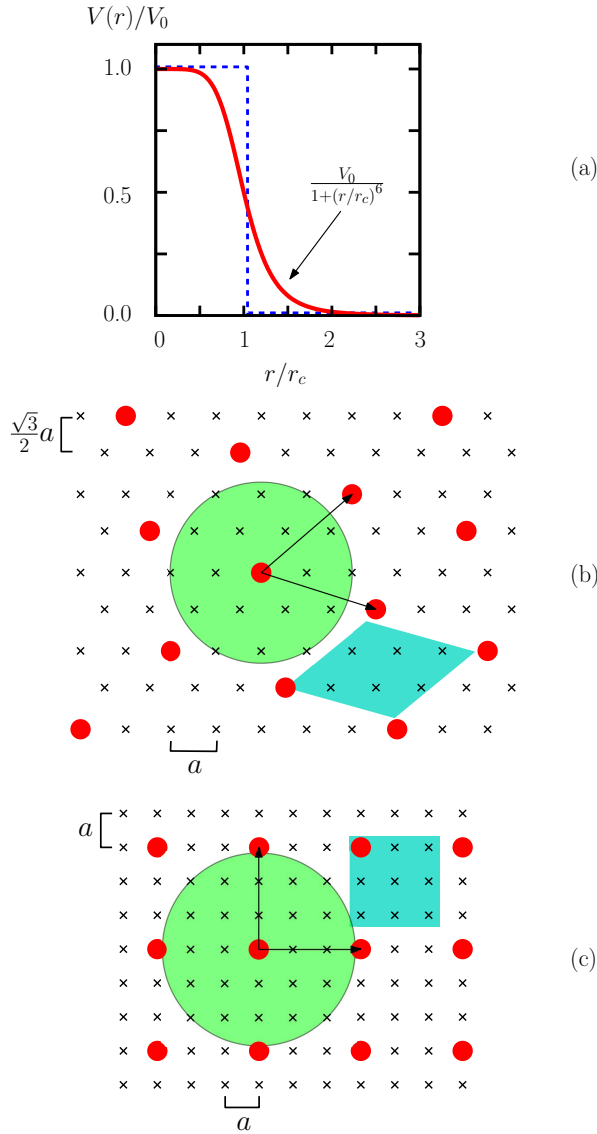


FIG. 1. Panel (a): examples of extended-range interactions. The continuous and dashed curves represent a soft-shoulder potential (see label) with fast-decaying (i.e., $(r/r_c)^{-6}$) tail and a shoulder interaction of strength V_0 and radius r_c , respectively. Single-particle crystalline ground states of the extended Bose-Hubbard Hamiltonian in Eq. (1) on a triangular lattice for $r_c = 2a$ and $\rho = 1/7$ [panel (b)], and on a square lattice for $r_c = 2\sqrt{2}a$ and $\rho = 1/9$ [panel (c)]. In panels (b) and (c), black crosses are lattice sites and red dots are occupied sites. Green circles highlight the range of the interaction around an occupied site, black arrows are the vectors generating the crystalline structure, and cyan regions indicate the primitive cells of the crystals.

rium phases. Our main findings are the following: i) As opposed to the isotropic and anisotropic supersolid GS's, a low-temperature quench leads to largely isotropic, OOE (super)solid states. Remarkably, these are also found for values of V at which the equilibrium phases are instead anisotropic. ii) Similarly to our previous study of the

same (albeit with smaller r_c) quantum model on the triangular lattice [27], as well as to that of the classical model in free space [17], the OOE counterpart of the equilibrium crystal at large V is a normal glass. iii) In the investigated parameter range no evidence of superglassy behavior is obtained. The occurrence of such a state, which has been predicted for the triangular lattice, crucially depends on the interplay between lattice geometry, particle density and inter-particle interactions.

The remainder of this paper is organized as follows: in the next section we describe the details of the hamiltonian model of our interest with particular attention to its cluster-forming regimes and, briefly, the numerical method adopted to carry out our investigation. In Section III we present and discuss our results, while in the last section we outline the conclusions of our work.

II. MODEL AND METHODS

The model we investigate is described by the Hamiltonian

$$H = -t \sum_{\langle ij \rangle} (b_i^\dagger b_j + \text{h.c.}) + V \sum_{i < j: r_{ij} \leq r_c} n_i n_j \quad (1)$$

on a square lattice of $N = L \times L$ sites and lattice constant a with periodic boundary conditions. Here t is the hopping coefficient between nearest-neighbor sites, b_i and b_i^\dagger are annihilation and creation operators for hardcore bosons on site i , respectively, $n_i = b_i^\dagger b_i$, V is the interaction strength and r_{ij} is the distance between sites i and j . In the following, a and t will be taken as units of length and energy, respectively.

For $r_c = a$, i.e. nearest-neighbor potential, the phase diagram of the model contains superfluid, solid, and insulating phases [29], while supersolid states can be stabilized adding longer-ranged density-density interactions [30, 31]. We study the model for $r_c > a$, in a regime where cluster formation takes place in the system.

For low enough ρ , the classical (i.e., $t = 0$) GS is a zero-energy single-particle crystal, where the inter-particle spacing is larger than the interaction radius. The maximum density ρ_c for which such a crystal exists is determined by r_c and the lattice geometry. For example, in our study of Eq. (1) on the triangular lattice the choice $r_c = 2a$ results in a critical density $\rho_c^{\text{tr}} = 1/7$. In the equilibrium study performed in [28], on the other hand, a square lattice geometry with $r_c = 2\sqrt{2}a$ leads to a critical density $\rho_c^{\text{sq}} = 1/9$. The single-particle crystalline structures corresponding to these densities are shown in Fig. 1(b-c), respectively.

For $\rho \gtrsim \rho_c$, a single-particle solid has a higher potential energy than a solid in which particles group up in tightly packed clusters. Indeed, the latter can arrange themselves far enough from each other to be noninteracting (i.e., outside of their mutual interaction radius). A

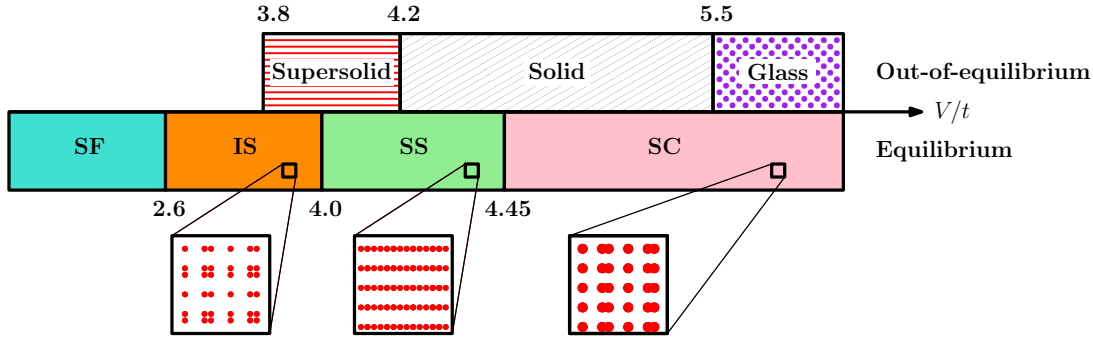


FIG. 2. Schematic phase diagram of Eq. (1) as a function of the interaction strength V/t . Each colored region in the lower part of the figure corresponds to a GS equilibrium phase: namely, a superfluid (SF, cyan), an isotropic supersolid (IS, orange), a stripe supersolid (SS, green) and a stripe crystal (SC, pink). The drawings are sketches of the crystalline structure (where present) of each equilibrium phase. The filling patterns in the upper part of the diagram identify the OOE states reached via simulated temperature quenching at target temperature $T/t = 1/20$. The regions where quenching leads to OOE supersolid, solid and glassy states are denoted by horizontal, diagonal or dot filling patterns, respectively.

larger value of ρ results in the formation of larger clusters. For instance, on the triangular lattice the chosen value of $\rho = 13/36 \sim 2.5\rho_c^{\text{tr}}$ led to clusters of $3 \div 4$ particles on average, while on the square lattice, for $\rho = 5/36 \sim 1.25\rho_c^{\text{sq}}$, the largest clusters contain 2 particles.

When the system is driven away from thermal equilibrium, cluster formation can cause effective polydispersity, which in turn plays a fundamental role in the appearance of (super)glassy states [27]. This phenomenon is favored by large cluster sizes, as well as (sufficiently) strong interactions, which prevent particles from delocalizing between different clusters, as well as entire clusters from spatially rearranging to establish an ordered (crystalline) structure.

In this work we analyze the OOE physics of Eq. (1) for the same parameter range investigated in [28]. The model shows a rich GS phase diagram, characterized by, e.g., competing supersolid phases. Understanding how temperature quenching may alter this scenario is one of the main objectives of the present study. Furthermore here, due to the presence of significantly smaller clusters, frustration effects should be significantly weaker than those occurring in the study of Ref. [27] on the triangular lattice. This would allow to determine, for instance, to which degree various OOE phenomena depend on clusterization.

We study the model Eq. (1) by means of Path Integral Quantum Monte Carlo simulations using Worm updates [32]. This technique yields numerically exact results for unfrustrated bosonic systems and allows to accurately estimate observables such as the superfluid fraction $\rho_s/\rho = (4\beta t\rho)^{-1} \langle W_x^2 + W_y^2 \rangle$ and the static structure factor $S(\mathbf{k}) = N^{-2} \sum_{ij} \exp[-i\mathbf{k}(\mathbf{r}_i - \mathbf{r}_j)] \langle n_i n_j \rangle$. These order parameters measure superfluidity and crystalline order, respectively, and are defined in terms of the inverse temperature $\beta = (k_B T)^{-1}$ (k_B is the Boltzmann constant, set to 1 in the following), of the winding number W_x, W_y in direction x, y , respectively, and of the lattice wavevectors \mathbf{k} . Here, $\langle \dots \rangle$ stands for statistical average.

We also estimate the renormalized Edwards-Anderson parameter $Q_{\text{EA}} = \sum_i \langle n_i - \rho \rangle^2 / Q_{\text{EA}}^0$, a well-known observable which allows to identify glass behavior in lattice systems in the absence of crystalline order. The normalization $Q_{\text{EA}}^0 = N\rho(1-\rho)$ is the value obtained for a fully localized state. Finally, we determine the single-particle Green Function defined as $G(\mathbf{r}) = N^{-1} \sum_i \langle b_i^\dagger b_{i+\mathbf{r}} \rangle$, associated to the presence of off-diagonal quasi-long range order in our two-dimensional system.

We perform large-scale simulations with up to $N = 96 \times 96$ sites and temperatures between $T/t = 1$ and $T/t = 1/20$, the latter yielding essentially GS results in the equilibrium case [28]. To gain insight into the OOE scenarios, we employ a simulated quench protocol, by running low- T simulations starting from high- T configurations without performing simulated annealing steps in T .

III. RESULTS

For clarity, we begin our discussion by summarizing the GS phase diagram of model Eq. (1) (we refer the reader to Ref. [28] for an exhaustive discussion). The GS (lower part of Fig. 2) is a superfluid (SF) at weak interactions, which makes way for an isotropic supersolid (IS) at $V/t = 2.6$. The system then undergoes a first-order transition at $V/t = 4.0$ to a supersolid state with anisotropic stripe crystalline structure and superfluid response, i.e., a stripe supersolid (SS). Finally, superfluidity is lost at $V/t = 4.45$, and the GS becomes a stripe crystal (SC).

Driving the system away from thermal equilibrium results in the OOE phase diagram shown in the upper part of Fig. 2, obtained via analysis of the relevant observables shown in Figs. 3, and 4 and discussed below. In the strongly interacting regime, i.e., $V/t > 5.5$, and for temperatures $T/t < 1/5$, the simulated quenches stabi-

lize OOE states where diagonal long range order vanishes in the thermodynamic limit. As signaled by the finite value of Q_{EA} (see Fig. 3), concomitant to the absence of superfluidity, the resulting states are normal glasses. Conversely, following our quenches at $T/t = 1/20$ in the intermediate- V/t region (i.e., $3.8 \leq V/t \leq 4.6$) the system retains long range order, reaching OOE states with crystalline structures different from those obtained at equilibrium [see Fig. 4(d)]. These results allow to identify a variety of crystalline states in the OOE phase diagram. For $V/t < 4.2$ the system displays superfluid behavior [see Fig. 4(c)]. The latter coexists with diagonal long range order down to $V/t = 3.8$, pointing out the occurrence of OOE supersolid states in this parameter region. For $V/t < 3.8$ our quenching process is ineffective, and the system equilibrates to an IS and a SF for $V/t > 2.6$ and $V/t < 2.6$, respectively. Remarkably, the OOE supersolids display features considerably different from their equilibrium counterparts. Specifically, both superfluid responses and crystalline order are essentially isotropic even when the corresponding equilibrium supersolids are strongly anisotropic.

In both the high- and intermediate- V/t region, we determine the degree of equilibration of each simulated quench by performing it in several (i.e., $\gtrsim 30$) independent realizations, differing in both the initial configuration and in the thermalization seed of the QMC simulation. If our quench protocol is not sufficient to drive the system away from thermal equilibrium, essentially all the realizations will converge to the equilibrium state, since the details of the QMC stochastic dynamics in configuration space do not matter in this case. On the other hand, where the OOE driving succeeds most of the realizations fail to equilibrate, with their initial conditions becoming crucial in determining the state reached by each simulation. A typical example of the latter behavior is shown in Fig. 3(a), where the mean value of an observable (in this case, the maximum value of the structure factor $S_{\text{max}}^{(R)}$) strongly depends on the realization.

Figure 3(b-d) show the scaling, as a function of the system size, of the realization-averaged maximum peak of the structure factor S_{max} and of the EA parameter Q_{EA} after quenching to different target temperatures for $V/t = 5.0$ and $V/t = 6.0$ (filled and empty symbols, respectively). For these values of V/t , the observed OOE states are non-superfluid. We find equilibration to a stripe solid for $T/t = 1/5$ (triangles). A decrease of the target temperature results in failure to equilibrate the vast majority of realizations, which converge to states where diagonal long range order is suppressed with respect to the equilibrium scenario. For $V/t = 5.0$, S_{max} remains finite in the thermodynamic limit for $T/t = 1/10$ (filled squares) and $T/t = 1/20$ (filled circles), signaling an OOE crystal. Conversely, crystalline order is lost for $V/t = 6.0$ and $T/t = 1/10$ (empty squares) and $T/t = 1/20$ (empty circles). For these temperatures, Q_{EA} remains finite [panel (d)], signaling the emergence of glassy behavior.

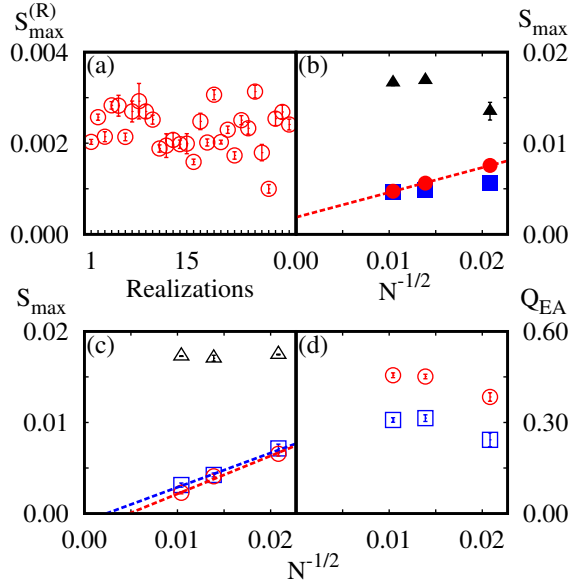


FIG. 3. Results for finite-temperature simulated quenches performed at $V/t = 5.0$ and $V/t = 6.0$. Panel (a): maximum value of the structure factor $S_{\text{max}}^{(R)}$ as a function of the realization index for $L = 96$, $T/t = 1/20$, and $V/t = 6.0$. Panel (b): realization-averaged value of S_{max} as a function of the inverse system size for $V/t = 5.0$. Panel (c): same as for panel (b) for $V/t = 6.0$. Panel (d): Edwards-Anderson parameter Q_{EA} as a function of the inverse system size for $V/t = 6.0$. In all panels, filled (empty) symbols correspond to $V/t = 5.0$ ($V/t = 6.0$), while triangles, squares and circles correspond to $T/t = 1/5, 1/10, 1/20$, respectively. The dashed lines correspond to linear fits in $N^{-1/2}$, shown when estimates for the two largest sizes are not identical within numerical uncertainty.

Figure 4 shows a detailed comparison of the superfluid and crystalline order parameters for the OOE and equilibrium cases (full and empty symbols, respectively) as a function of V/t . Supersolid behavior occurs, after quenching, for $3.8 \leq V/t < 4.2$, i.e., in an interaction strength window smaller than that for which supersolidity is found at equilibrium. In particular, superfluidity vanishes in the thermodynamic limit for $V/t \geq 4.2$ (diamonds in Fig. 4(b)). More importantly, the features of these supersolid OOE states may be both quantitatively and qualitatively different from the equilibrium ones, whose order parameters are denoted for clarity by ρ_s^{eq}/ρ and $S_{\text{max}}^{\text{eq}}$, respectively. As expected, for small $V/t \lesssim 4$ our quenching protocol does not significantly alter the values of ρ_s/ρ and S_{max} with respect to ρ_s^{eq}/ρ and $S_{\text{max}}^{\text{eq}}$ [Fig. 4(c-d) and finite-size scaling for $V/t = 3.9$ (triangles in panels (a) and (b))]. For intermediate V/t , while at the IS/SS transition $S_{\text{max}}^{\text{eq}}$ (empty squares in Fig. 4(d)) develops strong anisotropy [28] and features a sizeable variation, S_{max} remains essentially constant (filled squares in Fig. 4(d)) and isotropic. Indeed, in all quench realizations the maximum peaks of the structure factor occur at realization-dependent

wavevectors $(k_x^{(R)}, 0)$ and $(0, k_y^{(R)})$ with $k_x^{(R)} \simeq k_y^{(R)}$ and $S^{(R)}(k_x^{(R)}, 0) \simeq S^{(R)}(0, k_y^{(R)})$. Similarly, ρ_s/ρ (filled circles in Fig. 4(c)) takes considerably lower values than ρ_s^{eq}/ρ (empty circles in Fig. 4(c)) for $V/t \gtrsim 4.0$ and the superfluid response, as opposed to what found at equilibrium, is essentially isotropic. This clarifies the difference between the equilibrium supersolid states, which can be either isotropic or anisotropic, and the OOE ones, which are found to be always largely isotropic. Such a difference persists even in the absence of superfluidity in the OOE states: for example, for $V/t > 4.45$ the GS is a stripe crystal while quenching results in the appearance of substantially isotropic crystals and glasses.

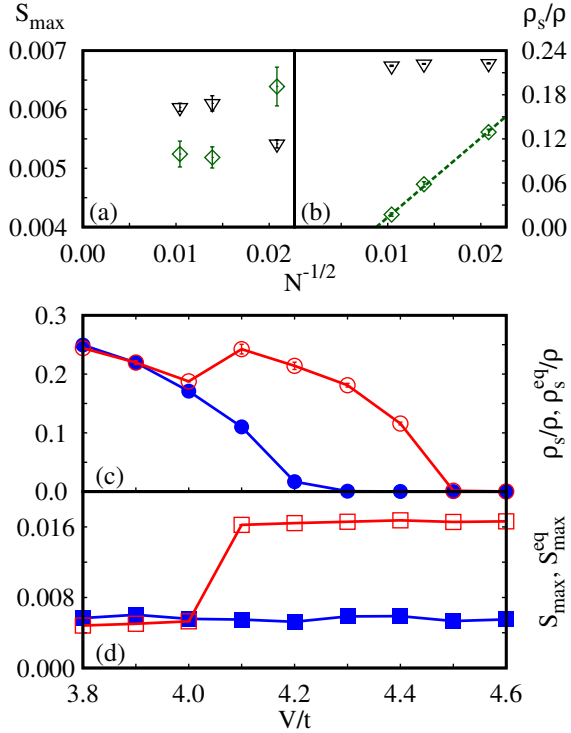


FIG. 4. Panels (a),(b): scaling in the inverse size of ρ_s/ρ and S_{max} for $V/t = 3.9$ (triangles) and $V/t = 4.2$ (diamonds) at $T/t = 1/20$. Dashed lines are linear fits to the numerical data, shown when estimates for the two largest sizes are not identical within their uncertainty. Panel (c): comparison between the equilibrium superfluid fraction ρ_s^{eq}/ρ (empty circles) and the OOE one ρ_s/ρ (filled circles) as a function of the interaction strength at $T/t = 1/20$, and $L = 96$. Panel (d): comparison of the equilibrium maximum value of the structure factor $S_{\text{max}}^{\text{eq}}$ (empty squares) and the OOE one S_{max} (filled squares) for the same parameters of panel (c). In panels (c) and (d), solid lines are guides to the eye.

The isotropic character of the OOE states can also be inferred by inspection of G_x and G_y , i.e., the single-particle Green Function $G(\mathbf{r})$ along the x and y directions, respectively. For $V/t = 4.1$, G_x and G_y of the corresponding anisotropic SS ground-state (triangles and circles in Fig. 5(a), respectively) are clearly different.

Specifically, while both decay algebraically as a function of the distance, signaling quasi-off-diagonal long range order, G_y is characterized by oscillations in correspondence of the stripe periodicity. The OOE $G(\mathbf{r})$, on the other hand, is essentially isotropic, i.e., $G_x \sim G_y$ (squares in Fig. 5(a)).

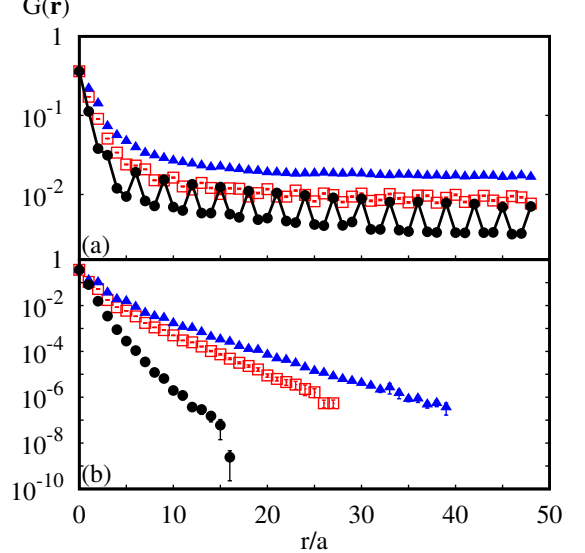


FIG. 5. Panel (a): single-particle Green function $G(\mathbf{r})$ for $T/t = 1/20$, $L = 96$, and $V/t = 4.1$. Triangles and circles refer to the equilibrium $G(\mathbf{r})$ along the x and y direction, respectively (see text), while squares denote the OOE $G(\mathbf{r})$ along the y direction. The corresponding OOE $G(\mathbf{r})$ along the x direction (not shown) is essentially identical. Continuous lines are guides to the eye. Panel (b): same as panel (a) for $V/t = 6.0$.

Fig. 5(b) displays the same comparison for $V/t = 6.0$. Here the decay of the $G(\mathbf{r})$, both at equilibrium and OOE, is exponential, as expected for a nearly classical crystal and a glass, respectively. Also in this case, the equilibrium $G(\mathbf{r})$ is strongly anisotropic, while $G_x \sim G_y$ in its OOE counterpart.

Further insight into the OOE physics of our model can be gained from the averaged occupation maps in Fig. 6. In both cases shown in figure [$V/t = 6.0$ in panel (a) and $V/t = 4.1$ in panel (b)] particles clusterize; for strong V/t , clusters have in general different shapes and orientations. These induce an effective polidispersity, ultimately resulting in glassy behavior [17]. On the other hand, for $V/t = 4.1$, where the system is supersolid, particles can “hop” between different clusters, establishing long exchange cycles which give rise to a sizeable superfluid response. The latter is concomitant with a well defined crystalline structure.

It is important to mention that no evidence of superglassy behavior has been found in the parameter range investigated in this work. This constitutes an important difference with the results of our recent study of model Eq. (1) for $r_c = 2$ on the triangular lattice [27].

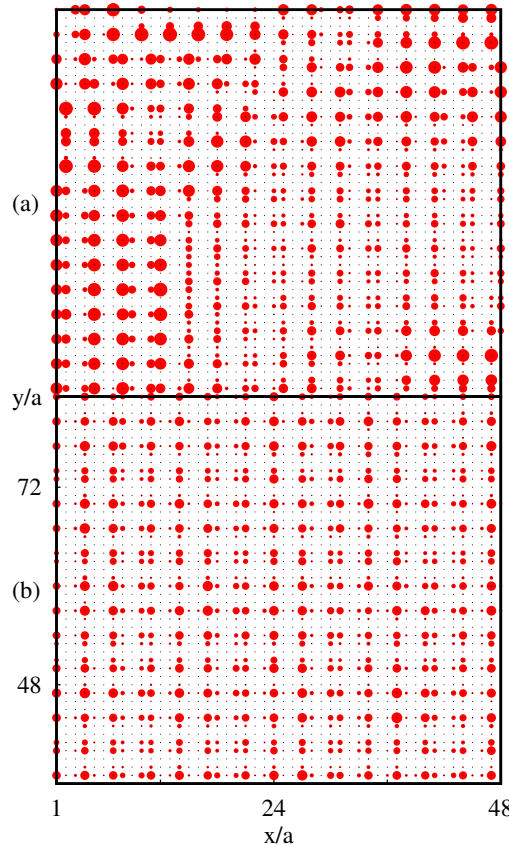


FIG. 6. Panel (a): portion of a site occupation map for one realization for $L = 96$, $T/t = 1/20$, and $V/t = 6.0$. Panel (b): same as panel (a) for $V/t = 4.1$. In both panels, black dots correspond to lattice sites, while the size of the red dot on each site is proportional to its occupation.

A qualitative explanation can be given in terms of a simple energetic argument. Indeed, the ratio Λ between potential and kinetic energy can be used to roughly estimate particle mobility. When Λ is large, i.e., for large V/t , particles, and clusters formed after quenching, are strongly localized, preventing the realization of a crystalline structure. Superglassy behavior emerges as a delicate balance between localization and superfluidity, which conversely takes place, at low T/t , for small Λ .

Indeed, on the triangular lattice superglasses were observed as the OOE counterparts of supersolids at $\Lambda \sim 9$ and $\rho_s/\rho \sim 0.1$. On the other hand, the equilibrium supersolid phases of model Eq. (1) on the square lattice are characterized by much smaller $\Lambda \sim 1.1 \div 1.3$ and higher $\rho_s/\rho \sim 0.2$. Here the OOE driving leads to superfluid states where, due to larger mobility, crystalline order can

be restored.

IV. CONCLUSIONS AND OUTLOOK

We study the out-of-equilibrium scenarios of a model of monodispersed hard-core bosons on a square lattice with an extended-range potential of the soft-shoulder type, of interest for experiments with cold Rydberg-dressed atoms. In the parameter region of our investigation, the ground state of the model is a cluster crystal and a superfluid for strong and weak interactions respectively, and a rare transition between an isotropic and an anisotropic supersolid state occurs for intermediate interaction strength.

Via simulated temperature quenches, we obtain a glass region for strong interactions, while for moderate values of the latter a supersolid region appears. We show that such a supersolid is qualitatively different from the ground state one, being essentially isotropic even for values of the interaction strength for which the corresponding ground state is anisotropic.

For all interaction strength values where out-of-equilibrium superfluidity remains finite, long range crystalline order is also maintained. Therefore, no evidence of superglassy behavior is found in our region of investigation, as opposed to the case of the triangular lattice, where we demonstrated such an exotic state. This discrepancy can be qualitatively explained in terms of the strong difference in the potential to kinetic energy ratio, which takes significantly different values on the two mentioned lattice geometries. In particular, this quantity is considerably smaller on the square lattice, signaling increased particle mobility. The latter suppresses particle and cluster localization, which is an essential ingredient for the onset of glassy physics.

V. ACKNOWLEDGEMENTS

We acknowledge useful discussion with A. Kuklov, W. Lechner, M. Mattioli, and S. Wessel. Work in Strasbourg was supported by the grant ANR-ERA-NET QuantERA - Projet RouTe (ANR-18-QUAN-0005-01). G. P. acknowledges support from the Institut Universitaire de France (IUF) and USIAS. G. M. was also supported by the French National Research Agency (ANR) through the Programme d'Investissement d'Avenir under contract ANR-17-EURE-0024. T. Y. was also supported by the National Natural Science Foundation of China (No. 11504067). Work in Trieste was supported by the ERC under grant number 758329 (AGEnTh) and by the EU Quantum Flagship grant PASQuanS.

[1] M. Boninsegni and N. V. Prokof'ev, Rev. Mod. Phys. **84**, 759 (2012).

[2] R. Nandkishore and D. A. Huse, Annual Review of Condensed Matter Physics **6**, 15 (2015).

- [3] X.-L. Qi and Z. S.-C., Physics Today **63**, 33 (2010).
- [4] S. F. Edwards and P. W. Anderson, Journal of Physics F: Metal Physics **5**, 965 (1975).
- [5] K. Binder and A. P. Young, Rev. Mod. Phys. **58**, 801 (1986).
- [6] B. M. Mladek, D. Gottwald, G. Kahl, M. Neumann, and C. N. Likos, Phys. Rev. Lett. **96**, 045701 (2006).
- [7] D. A. Lenz, R. Blaak, C. N. Likos, and B. M. Mladek, Phys. Rev. Lett. **109**, 228301 (2012).
- [8] E. Sciortino, Francesco; Zaccarelli, Nature **493**, 30 (2013).
- [9] M. Saffman, T. Walker, and K. Mølmer, Rev. Mod. Phys. **82**, 2313 (2010).
- [10] Y.-Y. Jau, A. M. Hankin, T. Keating, I. H. Deutsch, and G. W. Biedermann, Nature Physics **12**, 71 (2015).
- [11] J. Zeiher, R. van Bijnen, P. Schauß, S. Hild, J. yoon Choi, T. Pohl, I. Bloch, and C. Gross, Nature Physics **12**, 1095 (2016).
- [12] T. Lahaye, C. Menotti, L. Santos, M. Lewenstein, and T. Pfau, Rep. Prog. Phys. **72**, 126401 (2009), 0905.0386.
- [13] R. Löw, H. Weimer, J. Nipper, J. B. Balewski, B. Butscher, H. P. Büchler, and T. Pfau, J. Phys. B **45**, 113001 (2012).
- [14] H. Bernien, S. Schwartz, A. Keesling, H. Levine, A. Omran, H. Pichler, S. Choi, A. S. Zibrov, M. Endres, M. Greiner, V. Vuletić, and M. D. Lukin, Nature **551**, 579 (2017).
- [15] S. de Lsleuc, V. Lienhard, P. Scholl, D. Barredo, S. Weber, N. Lang, H. P. Bchler, T. Lahaye, and A. Browaeys, arXiv:1810.13286.
- [16] R. Díaz-Méndez, F. Mezzacapo, F. Cinti, W. Lechner, and G. Pupillo, Phys. Rev. E **92**, 052307 (2015).
- [17] R. Díaz-Méndez, F. Mezzacapo, W. Lechner, F. Cinti, E. Babaev, and G. Pupillo, Phys. Rev. Lett. **118**, 067001 (2017).
- [18] R. Diaz-Mendez, G. Pupillo, F. Mezzacapo, M. Wallin, J. Lidmar, and E. Babaev, Soft Matter **15**, 355 (2019).
- [19] M. Mattioli, M. Dalmonte, W. Lechner, and G. Pupillo, Phys. Rev. Lett. **111**, 165302 (2013).
- [20] M. Dalmonte, W. Lechner, Z. Cai, M. Mattioli, A. M. Läuchli, and G. Pupillo, Phys. Rev. B **92**, 045106 (2015).
- [21] M. Motta, E. Vitali, M. Rossi, D. E. Galli, and G. Bertaina, Phys. Rev. A **94**, 043627 (2016).
- [22] M. Teruzzi, D. E. Galli, and G. Bertaina, Journal of Low Temperature Physics **187**, 719 (2017).
- [23] N. Henkel, R. Nath, and T. Pohl, Phys. Rev. Lett. **104**, 195302 (2010).
- [24] N. Henkel, F. Cinti, P. Jain, G. Pupillo, and T. Pohl, Phys. Rev. Lett. **108**, 265301 (2012).
- [25] F. Cinti, P. Jain, M. Boninsegni, A. Michel, P. Zoller, and G. Pupillo, Phys. Rev. Lett. **105**, 135301 (2010).
- [26] F. Cinti, T. Macrì, W. Lechner, G. Pupillo, and T. Pohl, Nature communications **5** (2014).
- [27] A. Angelone, F. Mezzacapo, and G. Pupillo, Phys. Rev. Lett. **116**, 135303 (2016).
- [28] G. Masella, A. Angelone, F. Mezzacapo, G. Pupillo, and N. V. Prokof'ev, Phys. Rev. Lett. **123**, 045301 (2019).
- [29] G. Schmid, S. Todo, M. Troyer, and A. Dorneich, Phys. Rev. Lett. **88**, 167208 (2002).
- [30] G. G. Batrouni and R. T. Scalettar, Phys. Rev. Lett. **84**, 1599 (2000).
- [31] F. Hébert, G. G. Batrouni, R. T. Scalettar, G. Schmid, M. Troyer, and A. Dorneich, Phys. Rev. B **65**, 014513 (2001).
- [32] N. V. Prokof'ev, B. V. Svistunov, and I. S. Tupitsyn, Journal of Experimental and Theoretical Physics **87**, 310 (1998).